Amplifying a Zeptonewton Force with a Single-Ion Nonlinear Oscillator

Bo Deng[1], Moritz Göb[1], Benjamin A. Stickler[2,3], Max Masuhr[1], Kilian Singer[1,*] and Daqing Wang[1,†]

[1]*Institute of Physics, University of Kassel, Heinrich-Plett-Straße 40, 34132 Kassel, Germany*
[2]*Institute for Complex Quantum Systems, Ulm University, Albert-Einstein-Allee 11, 89069 Ulm, Germany*
[3]*Faculty of Physics, University of Duisburg-Essen, Lotharstraße 1, 47057 Duisburg, Germany*

Nonlinear mechanical resonators display rich and complex dynamics and are important in many areas of fundamental and applied sciences. Here, we present a general strategy to generate mechanical nonlinearities for trapped particles by transverse driving in a funnel-shaped potential. Employing a trapped ion platform, we study the nonlinear oscillation, bifurcation, and hysteresis of a single calcium ion and demonstrate a 20-fold enhancement of the signal from a zeptonewton-magnitude harmonic force through the effect of vibrational resonance. Our results represent a first step in combining the rich nonlinear dynamics with the precision control over mechanical motions offered by atomic physics and open up possibilities for exploiting nonlinear mechanical phenomena in the quantum regime.

Nonlinear oscillators, whose dynamics go beyond the simple description of simple equations of motion, are ubiquitous in nature. Driven nonlinear oscillators can exhibit complex behaviors such as squeezing [1,2], persistent resonance [3], phase transitions [4–6], and chaos [7,8]. They have a broad presence in many branches of science and technology [9–15]. Compared to linear oscillators, nonlinear oscillators can be more sensitive to external forces, especially when they are tuned close to a bifurcation point. The multistability of nonlinear oscillators provides opportunities for signal enhancement through the effects of stochastic and vibrational resonances [16–20]. The manifestation of these effects in mechanical systems has primarily been investigated with clamped electromechanical resonators [17,18,20]. Engineering mechanical nonlinearities for single atoms trapped in ultrahigh vacuum would allow for the combination of nonlinear dynamics with the exquisite control over mechanical motion achievable by laser cooling and enable nonlinear force amplification on a new scale.

In this Letter, we present a strategy to create mechanical nonlinearities through transverse driving of a particle trapped in a funnel-shaped potential. This nonlinearity arises from the coupling of radial and axial motion of the particle imposed by the geometry of the potential [21,22]. We demonstrate this model experimentally using a single calcium ion confined in a funnel-shaped Paul trap and

report the first observation of force amplification through vibrational resonance in levitated systems. In particular, we show that a zeptonewton-scale oscillatory force, which displaces the ion by an amount comparable to its zero-point motion, can be enhanced by a factor of 20.

As illustrated in Fig. 1(a), our system consists of a single ion in a modified Paul trap. In contrast to conventional linear Paul traps, the two pairs of blade electrodes are inclined with respect to the axial z axis [21,22]. We perform numerical field simulations using the boundary element method [23] to obtain the electrostatic potential. As displayed in Fig. 1(b), this arrangement leads to a funnel-shaped potential in which the radial confinement becomes stronger with increasing axial position z. To trap a charged particle, the two pairs of blades are driven by bipolar radio frequency signals $\pm\tilde{V}_{\mathrm{rf}}$ at a frequency of 11 MHz. This creates a secular trapping potential in the radial directions for a $^{40}\mathrm{Ca}^+$ ion. The blue and red dots in Fig. 1(c) display the measured secular trapping frequencies along the two radial principal axes x and y as a function of z. The results can be well recovered by the linear relation $\omega_{x,y}(1 + z/\ell_0)$, with $\omega_{x,y} \simeq 2\pi \times \{1.14, 1.15\}$ MHz the trapping frequencies at $z = 0$ and $\ell_0 = 1.81$ mm a parameter describing the length of the funnel. In the axial direction, the ion is weakly confined by positive dc voltages (V_{dc}) applied on the two end caps, resulting in a trapping frequency of $\Omega \simeq 2\pi \times 100$ kHz.

The motion of the ion is subject to continuous damping in all three directions achieved through Doppler cooling using a laser red detuned to its $4^2S_{1/2} - 4^2P_{1/2}$ transition [see inset of Fig. 1(a)]. A second laser at 866 nm repumps the metastable $3^2D_{3/2}$ state to facilitate a closed-cycle transition. In addition to the damping, the x and z motion
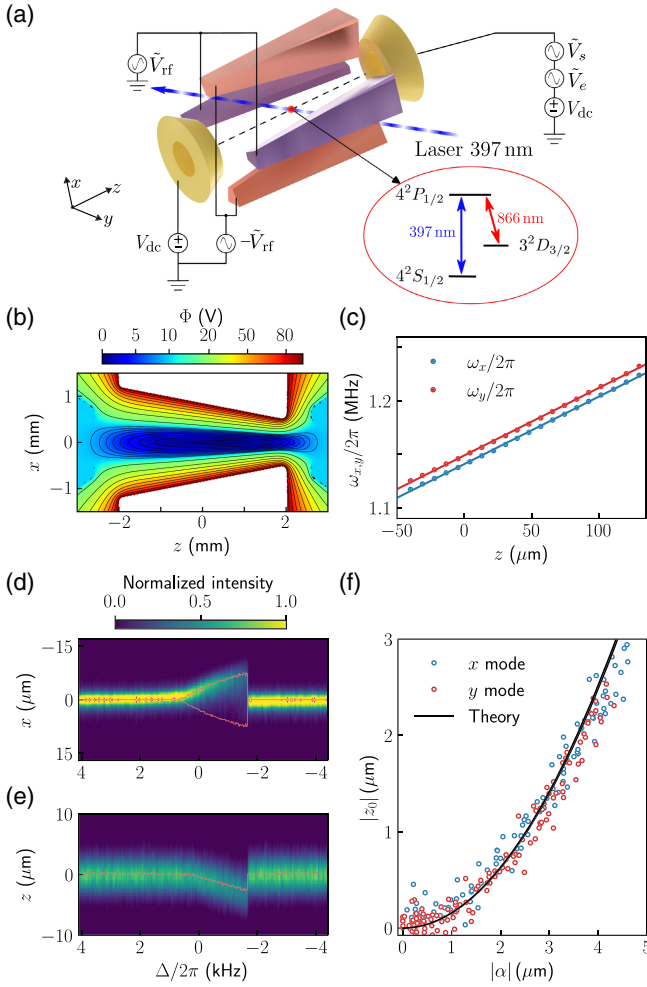
FIG. 1. (a) Experimental setup. Intensity modulation of the cooling laser excites the x mode of the ion. dc bias (V_{dc}) and two ac voltages ($\tilde{V}_s$, $\tilde{V}_e$) are applied to the end cap electrodes. Inset: a simplified energy level diagram for the ^{40}Ca$^+$ ion. (b) Electrostatic potential obtained from numerical simulations. (c) Dependence of radial trapping frequencies on the axial position. The dots represent measured data and the lines display linear fits. (d) Response of the x mode to a descending frequency sweep. Each column represents the projection of a fluorescence image along the z axis. The red lines display the extracted oscillation amplitude. (e) Response of the axial mode. The red line indicates the axial equilibrium position z_0. (f) The amplitude of axial displacement plotted against the radial oscillation amplitude. The solid line shows the predictions following Eq. (5) in the absence of $F_z(t)$.

are driven by external forces $F_x(t)$ and $F_z(t)$. Since the two radial modes are detuned in frequency by 8 kHz, narrow band modulation of the force F_x allows selective excitation of each radial mode. We consider that only the x mode is driven and set $y = 0$ for all times. In the relevant regime of the experiment, the impact of the funnel shape is weak, $|z/\ell_0| \ll 1$. Keeping the z dependence of the secular potential in linear order only, we obtain the Hamiltonian for the two-dimensional oscillation dynamics:

$$H = \frac{p_x^2 + p_z^2}{2m} + \frac{1}{2}m\Omega^2 z^2 + \frac{1}{2}m\omega_x^2\left(1 + 2\frac{z}{\ell_0}\right)x^2$$
$$- F_x(t)x - F_z(t)z. \tag{1}$$

Here, m represents the mass of the ^{40}Ca$^+$ ion. The driving forces have three distinct contributions: (i) F_x is realized by modulating the intensity of the cooling laser to produce a near-resonant radiation pressure force of magnitude F_0 and frequency $\omega_0 = \omega_x + \Delta \gg \Omega$ (with detuning Δ, $|\Delta| \ll \Omega$), which drives the x motion of the ion; (ii) a weak signal force of magnitude F_s and frequency $\omega_s \ll \omega_0$ acting on the axial mode, which we want to detect; (iii) the axial enhancement force of strength F_e and frequency ω_e, which serves to enhance the detection of the signal force F_s. In the experiment, the signal force is introduced by feeding in an ac voltage $\tilde{V}_s$ with an amplitude of 500 µV on one end cap electrode. The detection scheme is not limited to electrostatic forces and should be applicable to any interaction that leads to an axial displacement of the ion. The enhancement force is applied in the same manner by exerting an ac voltage $\tilde{V}_e$ on the same end cap electrode, as shown in Fig. 1(a). In summary, $F_x(t) = F_0\cos(\omega_0 t)$ and

$$F_z(t) = F_e\cos(\omega_e t) + F_s\cos(\omega_s t). \tag{2}$$

Note that the frequencies of these three forces fulfill the relation $\omega_s \ll \omega_e \ll \omega_0$, as required for vibrational resonance [19,20].

The equations of motion resulting from the Hamiltonian (1) can be simplified by exploiting the separation of timescales $\omega_0 \gg \Omega$. This is achieved by making the ansatz $x(t) = \alpha(t)e^{-i\omega_0 t} + \text{c.c.}$ (with c.c. the complex conjugate), where the amplitude α evolves on a timescale much slower than $1/\omega_0$, so that $|\ddot{\alpha}| \ll \omega_0|\dot{\alpha}|$ and $|\dot{\alpha}| \ll \omega_0|\alpha|$. Averaging over one drive period $2\pi/\omega_0$ and performing a rotating-wave approximation yields the approximate equation of motion for the radial mode,

$$\dot{\alpha} = i\left(\Delta - \omega_x\frac{z}{\ell_0}\right)\alpha + if_0 - \frac{\gamma}{2}\alpha, \tag{3}$$

with damping rate γ and driving strength $f_0 = F_0/4m\omega_x$. This equation shows that the axial displacement z shifts the resonance frequency of the radial oscillator by $\omega_x z/\ell_0$.

The axial motion is described by

$$\ddot{z} = -\Omega^2 z - \frac{2\omega_x^2}{\ell_0}|\alpha|^2 + \frac{F_z(t)}{m} - \gamma\dot{z}, \tag{4}$$

which follows from the exact equations of motion via the substitution $x^2 = 2|\alpha|^2$ due to the rotating-wave approximation. This equation implies that the instantaneous displacement of the axial equilibrium position,

$$z_0 = -2\frac{\omega_x^2}{\Omega^2}\frac{|\alpha|^2}{\ell_0} + \frac{F_z(t)}{m\Omega^2}, \quad (5)$$

is determined by the radial oscillation amplitude as well as by the external force (2). We note that micromotion at the trap radio frequency [24] introduces an extra displacement in the axial direction, which enters Eq. (5) in an additive manner. The amplitude of this displacement is 2 orders of magnitude smaller than that introduced by the secular motion and plays a minor role.

The coupling of radial and axial dynamics described by Eqs. (3) and (5) is key to the emergence of nonlinearity in this system. We verify this coupling by coherently driving the radial oscillator with the force F_x and observing the response in the axial direction. To do so, the modulation frequency of the cooling laser ω_0 is reduced stepwise across ω_x. In each step, a fluorescence image of the ion is recorded. The integration time of the camera is 400 ms. Each frame therefore averages over many axial and radial oscillation cycles. The images are then projected along the radial and axial axes to separate the responses along these two directions. The axial force F_z is not applied during this measurement. Figure 1(d) shows the response of the radial mode as a function of the frequency detuning Δ. As ω_0 approaches the resonance frequency, a coherent oscillation of the radial mode is excited. Here, only one flank of the oscillation is visible in the images due to a phase delay between the ion motion and the laser drive [25]. As the modulation frequency crosses ω_x, the coherent oscillation persists for an extended range. The increase of radial oscillation amplitude is accompanied with an axial shift in the negative direction of the z axis, i.e., the open end of the funnel, as displayed in Fig. 1(e). Narrow band intensity modulation of the cooling laser allows selective excitations of both x and y modes and quantitative comparison of the radial-axial coupling with Eq. (5). The results are displayed in Fig. 1(f). The slight mismatch between theory and experimental data at high oscillation amplitude is due to a reduced photon scattering rate and thus a smaller mean radiation pressure force as the ion moves out of the laser focus.

At further frequency detuning, the oscillator experiences an abrupt change in both the radial and axial directions and resumes its initial position. Such an abrupt change is a signature of bistability. Duffing-type bistability of trapped ions can arise from the intrinsic anharmonicity of linear Paul traps [26]. Here, the nonlinearity stems from the radial-axial coupling imposed by the funnel-shaped potential. This can be intuitively understood as shifting toward the open side of the funnel softens the radial spring and leads to an amplitude-dependent radial trapping frequency, i.e., a Duffing-type response [27].

To confirm the intuition, we solve the averaged radial amplitude equation (3). We use that the axial motion adiabatically follows the radial motion since $|\Delta| \ll \Omega$. One can thus average over one axial oscillation period $2\pi/\Omega$, replace z by z_0 in Eq. (3), and obtain

$$\dot\alpha = i[\Delta - \delta(t)]\alpha + i\xi|\alpha|^2\alpha + if_0 - \frac{\gamma}{2}\alpha. \quad (6)$$

This equation describes a Duffing oscillator with a linear drive f_0 and a parametric drive that modulates the detuning by $\delta(t) = \omega_x F_z(t)/m\ell_0\Omega^2$. Here, the parameter $\xi = 2\omega_x^3/\Omega^2\ell_0^2$ quantifies the nonlinearity due to the radial-axial coupling. In our experiment, $\xi/2\pi = 9.04 \times 10^{13}$ Hz/m^2 and significantly exceeds the intrinsic nonlinearity of the secular trapping potential.

Since the parametric driving frequencies [see Eq. (2)] are both much smaller than the damping rate, $\omega_s \ll \omega_e \ll \gamma$, the Duffing oscillator relaxes for each $\delta(t)$ toward a quasistationary state with the square of the amplitude $|\alpha_0(t)|^2$ determined by the third-order polynomial equation:

$$|\alpha_0(t)|^2 = \frac{f_0^2}{[\Delta - \delta(t) + \xi|\alpha_0(t)|^2]^2 + \gamma^2/4}. \quad (7)$$

The solutions of this equation as a function of the detuning Δ are displayed in Fig. 2(a). Depending on the driving strength, it has either a single stable solution or three
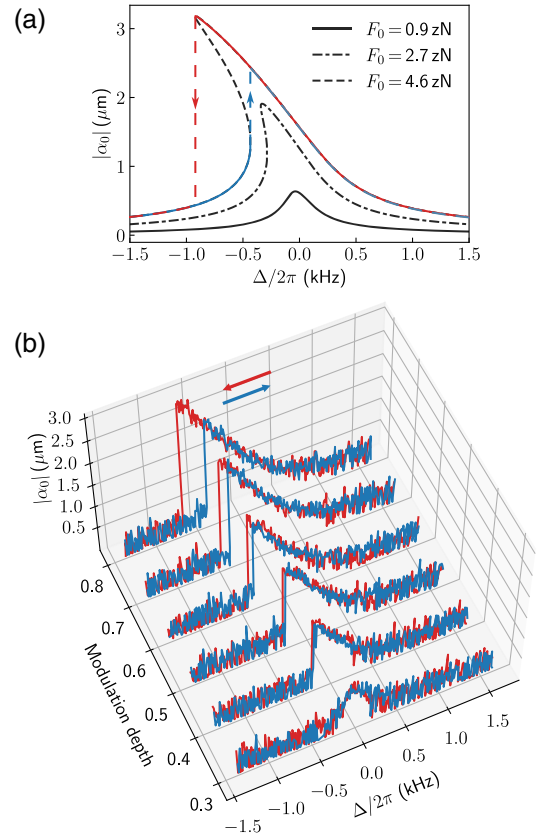
FIG. 2. (a) Solutions of $|\alpha_0|$ for $\gamma = 2\pi \times 250$ Hz and driving strengths denoted in the legend. (b) The emergence of bistability. The red lines show the radial amplitude when performing descending frequency sweeps and the blue lines represent the outcome for ascending sweeps.

stationary solutions, of which two are stable and one is unstable [27]. In the latter case, an adiabatic ramping of the detuning through the bistable region leads to hysteresis.

To verify the emergence of bistability, we gradually increase the modulation depth of the laser intensity, which increases the amplitude of the driving force. The results are displayed in Fig. 2(b). Under weak driving, the same Lorentzian-shaped response is observed for ascending (blue lines) and descending (red lines) sweeps. As the driving force increases, the line shape becomes unsymmetric and abrupt changes appear on the side of negative detuning. With stronger driving, the jumps occur at different frequency detunings for descending and ascending sweeps, confirming that $|\alpha_0|$ has more than one stable solution in this regime. As predicted by theory, the hysteresis region opens gradually as the driving force further increases.

Having characterized our system, we demonstrate that this nonlinear oscillator can be utilized for amplifying small signals through a scheme analogous to vibrational resonance [20]. To start, we exert the signal force F_s by switching on the ac voltage $\tilde{V}_s$ with an amplitude of 500 μV at frequency $\omega_s = 2\pi \times 0.5$ Hz [see Fig. 1(a) and the illustration in Fig. 3(a)]. In this step, the radial forcing is not applied ($F_x = 0$). The resulting signal force has a peak-to-peak amplitude of 2.4 zN and leads to a periodic displacement of ± 45 nm of the axial oscillator. This displacement is comparable to the zero-point fluctuation of the axial mode, which amounts to $\sqrt{\hbar/2m\Omega} \approx 36$ nm. We determine the axial trajectory of the ion through superresolution localization microscopy by performing a maximum likelihood estimation from the fluorescence images [28]. The resulting axial trajectory is displayed in the inset of Fig. 3(b). Here, the camera is sampled at about 8 Hz with an exposure time of 100 ms for each frame. On average, $N = 240$ photons are detected per frame. The experimental axial Gaussian spread function has a standard deviation of $\sigma_0 = 1.64$ μm and sets the lower bound of estimating the axial center position $\sigma_0/\sqrt{N} = 106$ nm [28]. The harmonic nature makes it possible to identify this signal in the Fourier domain. As shown in Fig. 3(b), a small peak at 0.5 Hz is barely visible in the Fourier spectrum.

Next, we force the radial oscillator to the bistable regime by switching on the radial driving F_x. The frequency ω_0 of the driving force is tuned to the center of the bistable region. The ion is initially prepared in the lower stable branch. The signal force F_s shifts the ion's motional state along the lower branch adiabatically but is too weak to induce a transition to the upper branch, as illustrated in Fig. 3(c). The measured axial trajectory and the corresponding Fourier spectrum are displayed in Fig. 3(d). The noise floor is elevated in the Fourier spectrum, but no enhancement of the signal at 0.5 Hz is observed.
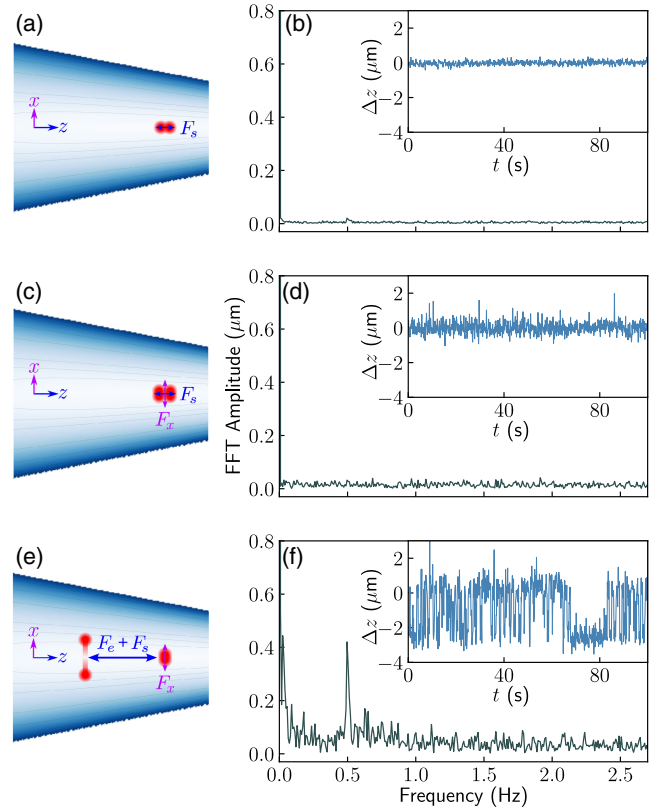

FIG. 3. Amplifying a weak signal force. (a) The weak signal force F_s is applied on the axial oscillator, introducing a small periodic axial displacement Δz which is barely visible in the Fourier spectrum displayed in (b). The inset shows the extracted axial center position as a function of time. (c) The radial drive F_x is applied. No enhancement is observed in the Fourier spectrum in (d). (e) The enhancement force F_e is switched on. The trajectory in the inset of (f) shows clearly jumps between the two stable branches. The Fourier spectrum in (f) has a prominent peak at 0.5 Hz.

In the last step, we apply a sinusoidal enhancement signal $\tilde{V}_e$ at $\omega_e = 2\pi \times 50$ Hz to one end cap, which exerts a parametric drive on the radial oscillator. The frequency of the enhancement force satisfies $\omega_s \ll \omega_e \ll \omega_0$ as required for vibrational resonance [19,20]. By tuning the amplitude of $\tilde{V}_e$ such that the parametric drive brings the oscillator to the boundaries of the bistable region, the signal force can introduce jumps of the oscillator to the upper branch and back [see Fig. 3(e)]. The inset of Fig. 3(f) shows the axial trajectory of the ion and clearly evidences the switch between two branches. In the Fourier spectrum, the strong peak at 0.5 Hz lets us deduce an enhancement factor of 20 compared to the signals in Figs. 3(b) and 3(d). The maximal amplification that can be achieved is determined by the width of the hysteresis region. In our experiment, this is limited by the saturation of the cooling transition, which sets an upper bound to the radial driving force.

In summary, we have shown that a single ion confined in a funnel-shaped potential exhibits a Duffing-type

nonlinearity. We demonstrated that this nonlinearity can be exploited to amplify a zeptonewton-scale oscillatory force. Our demonstration represents a first step in combining the rich dynamics of nonlinear oscillators with the exquisite control over mechanical motions offered by atomic physics and opens possibilities for studying and exploiting nonlinear mechanical phenomena in single and few-body systems close to their motional ground state. For instance, future work might assess the role of nonlinearity in energy transport through oscillator chains [29–31], study synchronization of driven nonlinear oscillators in the quantum regime [32,33], implement quantum sensing schemes by exploiting spin-motional coupling [34], explore the emergence of limit cycles [35], or investigate thermodynamics with quantum nonlinear oscillators [36]. The nonlinear force amplification scheme enables force detection in a broad low-frequency range with sensitivity at the zeptonewton level. This complements the established force detection schemes based on trapped ions, such as Doppler velocimetry [37] and injection locking [38], which achieve high sensitivity through operations close to the ion's mechanical resonances. The ability to enhance the detection of low-frequency periodic forces could be extended to study particles that are cotrapped with the atomic ion, such as cold neutral atoms [39–41] and molecular ions [42–44]. This would offer a promising route to detect forces that have not yet been observed on molecular systems, such as chiral optical forces [45–47], which are predicted to arise when placing chiral molecules in a helicity-gradient optical field and could reach the zeptonewton scale. Last but not least, the geometry-induced nonlinearity could also be exploited to generate nonclassical states of massive particles that lack sharp internal transitions, such as electrically levitated nanoparticles [48–50].

---

[*] ks@uni-kassel.de

[†] daqing.wang@uni-kassel.de

[1] F. Yang, M. Fu, B. Bosnjak, R. H. Blick, Y. Jiang, and E. Scheer, Phys. Rev. Lett. **127**, 184301 (2021).

[2] J. S. Huber, G. Rastelli, M. J. Seitner, J. Kölbl, W. Belzig, M. I. Dykman, and E. M. Weig, Phys. Rev. X **10**, 021066 (2020).

[3] F. Yang, F. Hellbach, F. Rochau, W. Belzig, E. M. Weig, G. Rastelli, and E. Scheer, Phys. Rev. Lett. **127**, 014304 (2021).

[4] C. Stambaugh and H. B. Chan, Phys. Rev. Lett. **97**, 110602 (2006).

[5] R. J. Dolleman, P. Belardinelli, S. Houri, H. S. van der Zant, F. Alijani, and P. G. Steeneken, Nano Lett. **19**, 1282 (2019).

[6] Q.-W. Wang and S. Wu, Phys. Rev. A **102**, 063531 (2020).

[7] J. Testa, J. Pérez, and C. Jeffries, Phys. Rev. Lett. **48**, 714 (1982).

[8] M. Lakshmanan and K. Murali, *Chaos In Nonlinear Oscillators: Controlling And Synchronization*, World Scientific Series On Nonlinear Science Series A, Vol. 13 (World Scientific Publishing Company, Singapore, 1996).

[9] S. H. Strogatz, *Nonlinear Dynamics and Chaos: With Applications to Physics, Biology, Chemistry, and Engineering*, 2nd ed. (CRC Press, Boca Raton, FL, 2015).

[10] Y. Tadokoro and H. Tanaka, Phys. Rev. Appl. **15**, 024058 (2021).

[11] A. N. Cleland and M. L. Roukes, J. Appl. Phys. **92**, 2758 (2002).

[12] J. Gieseler, L. Novotny, and R. Quidant, Nat. Phys. **9**, 806 (2013).

[13] L. Papariello, O. Zilberberg, A. Eichler, and R. Chitra, Phys. Rev. E **94**, 022201 (2016).

[14] Y. Zhang, R. Kondo, B. Qiu, X. Liu, and K. Hirakawa, Phys. Rev. Appl. **14**, 014019 (2020).

[15] S. Aldana, C. Bruder, and A. Nunnenkamp, Phys. Rev. A **90**, 063810 (2014).

[16] L. Gammaitoni, P. Hänggi, P. Jung, and F. Marchesoni, Rev. Mod. Phys. **70**, 223 (1998).

[17] R. L. Badzey and P. Mohanty, Nature (London) **437**, 995 (2005).

[18] R. Almog, S. Zaitsev, O. Shtempluck, and E. Buks, Appl. Phys. Lett. **90**, 013508 (2007).

[19] P. S. Landa and P. V. E. McClintock, J. Phys. A **33**, L433 (2000).

[20] A. Chowdhury, M. G. Clerc, S. Barbay, I. Robert-Philip, and R. Braive, Nat. Commun. **11**, 2400 (2020).

[21] J. Roßnagel, S. T. Dawkins, K. N. Tolazzi, O. Abah, E. Lutz, F. Schmidt-Kaler, and K. Singer, Science **352**, 325 (2016).

[22] A. Levy, M. Göb, B. Deng, K. Singer, E. Torrontegui, and D. Wang, New J. Phys. **22**, 093020 (2020).

[23] T. Betcke and M. W. Scroggs, J. Open Source Softwaare **6**, 2879 (2021).

[24] D. J. Berkeland, J. D. Miller, J. C. Bergquist, W. M. Itano, and D. J. Wineland, J. Appl. Phys. **83**, 5025 (1998).

[25] M. Drewsen, A. Mortensen, R. Martinussen, P. Staanum, and J. L. Sørensen, Phys. Rev. Lett. **93**, 243201 (2004).

[26] N. Akerman, S. Kotler, Y. Glickman, Y. Dallal, A. Keselman, and R. Ozeri, Phys. Rev. A **82**, 061402(R) (2010).

[27] A. H. Nayfeh and D. T. Mook, *Nonlinear Oscillations* (John Wiley & Sons, New York, 2008).

[28] M. Lelek, M. T. Gyparaki, G. Beliu, F. Schueder, J. Griffié, S. Manley, R. Jungmann, M. Sauer, M. Lakadamyali, and C. Zimmer, Nat. Rev. Methods Primers **1**, 39 (2021).

[29] Z. Zheng, G. Hu, and B. Hu, Phys. Rev. Lett. **86**, 2273 (2001).

[30] A. Kovaleva and L. I. Manevitch, Phys. Rev. E **88**, 022904 (2013).

[31] S. Borlenghi, S. Iubini, S. Lepri, L. Bergqvist, A. Delin, and J. Fransson, Phys. Rev. E **91**, 040102(R) (2015).

[32] S. Walter, A. Nunnenkamp, and C. Bruder, Phys. Rev. Lett. **112**, 094102 (2014).

[33] N. Lörch, E. Amitai, A. Nunnenkamp, and C. Bruder, Phys. Rev. Lett. **117**, 073601 (2016).

[34] P. A. Ivanov, N. V. Vitanov, and K. Singer, Sci. Rep. **6**, 28078 (2016).

[35] L. Ben Arosh, M. C. Cross, and R. Lifshitz, Phys. Rev. Res. **3**, 013130 (2021).

[36] U. C. Mendes, J. S. Sales, and N. G. de Almeida, J. Phys. B **54**, 175504 (2021).

[37] M. J. Biercuk, H. Uys, J. W. Britton, A. P. VanDevender, and J. J. Bollinger, Nat. Nanotechnol. **5**, 646 (2010).

[38] S. Knünz, M. Herrmann, V. Batteiger, G. Saathoff, T. W. Hänsch, K. Vahala, and T. Udem, Phys. Rev. Lett. **105**, 013004 (2010).

[39] P. Weckesser, F. Thielemann, D. Wiater, A. Wojciechowska, L. Karpa, K. Jachymski, M. Tomza, T. Walker, and T. Schaetz, Nature (London) **600**, 429 (2021).

[40] T. Feldker, H. Fürst, H. Hirzler, N. Ewald, M. Mazzanti, D. Wiater, M. Tomza, and R. Gerritsma, Nat. Phys. **16**, 413 (2020).

[41] J. Joger, H. Fürst, N. Ewald, T. Feldker, M. Tomza, and R. Gerritsma, Phys. Rev. A **96**, 030703(R) (2017).

[42] F. Wolf, Y. Wan, J. C. Heip, F. Gebert, C. Shi, and P. O. Schmidt, Nature (London) **530**, 457 (2016).

[43] C.-W. Chou, C. Kurz, D. B. Hume, P. N. Plessow, D. R. Leibrandt, and D. Leibfried, Nature (London) **545**, 203 (2017).

[44] K. Najafian, Z. Meir, M. Sinhal, and S. Willitsch, Nat. Commun. **11**, 4470 (2020).

[45] R. P. Cameron, S. M. Barnett, and A. M. Yao, New J. Phys. **16**, 013020 (2014).

[46] A. Canaguier-Durand, J. A. Hutchison, C. Genet, and T. W. Ebbesen, New J. Phys. **15**, 123037 (2013).

[47] B. A. Stickler, M. Diekmann, R. Berger, and D. Wang, Phys. Rev. X **11**, 031056 (2021).

[48] L. Martinetz, K. Hornberger, J. Millen, M. Kim, and B. A. Stickler, npj Quantum Inf. **6**, 101 (2020).

[49] L. Dania, D. S. Bykov, M. Knoll, P. Mestres, and T. E. Northup, Phys. Rev. Res. **3**, 013018 (2021).

[50] Y. Ren, E. Benedetto, H. Borrill, Y. Savchuk, M. Message, K. O'Flynn, M. Rashid, and J. Millen, Appl. Phys. Lett. **121**, 113506 (2022).